HHS Public Access

Author manuscript

Neuroimage. Author manuscript; available in PMC 2018 August 15.

Published in final edited form as:

Neuroimage. 2017 August 15; 157: 341–350. doi:10.1016/j.neuroimage.2017.06.007.

Enhancing sensitivity of pH-weighted MRI with combination of amide and guanidyl CEST

Tao Jin[1,2,*], **Ping Wang**[1], **T. Kevin Hitchens**[3], and **Seong-Gi-Kim**[4,5]

[1]Department of Radiology, University of Pittsburgh, Pittsburgh, PA

[2]Department of Bioengineering, University of Pittsburgh, Pittsburgh, PA

[3]Department of Neurobiology, University of Pittsburgh, Pittsburgh, PA

[4]Center for Neuroscience Imaging Research, Institute for Basic Science (IBS), Suwon, Korea

[5]Department of Biomedical Engineering, Sungkyunkwan University, Suwon, Korea

Abstract

Amide-proton-transfer weighted (APTw) MRI has emerged as a non-invasive pH-weighted imaging technique for studies of several diseases such as ischemic stroke. However, its pH-sensitivity is relatively low, limiting its capability to detect small pH changes. In this work, computer simulations, protamine phantom experiments, and *in vivo* gas challenge and experimental stroke in rats showed that, with judicious selection of the saturation pulse power, the amide-CEST at 3.6 ppm and guanidyl-CEST signals at 2.0 ppm changed in opposite directions with decreased pH. Thus, the difference between amide-CEST and guanidyl-CEST can enhance the pH measurement sensitivity, and is dubbed as pH_{enh}. Acidification induced a negative contrast in APTw, but a positive contrast in pH_{enh}. *In vivo* experiments showed that pH_{enh} can detect hypercapnia-induced acidosis with about 3-times higher sensitivity than APTw. Also, pH_{enh} reduced gray and white matter contrast compared to APTw. In stroke animals, the CEST contrast between the ipsilateral ischemic core and contralateral normal tissue was −1.85 ± 0.42% for APTw and 3.04 ± 0.61% (n = 5) for pH_{enh}, and the contrast to noise was 2.9 times higher for pH_{enh} than APTw. Our results suggest that pH_{enh} can be a useful tool for non-invasive pH-weighted imaging.

Keywords

CEST; amide; guanidyl; pH; APT; stroke

[*]Corresponding author: Tao Jin, Ph. D., Department of Radiology, University of Pittsburgh, 3025 E Carson Street, Room 156, Pittsburgh, PA, 15203, taj6@pitt.edu, (Tel) 412-383-8010, (Fax) 412-383-6799.

Introduction

The homeostasis of intracellular pH (simply referred to as pH hereafter) is essential for normal cellular functions and plays a vital role in cell physiology. Transient fluctuation in local tissue pH has been reported during neuronal activation, seizure and spreading depression (Autio et al., 2014; Chesler, 2003; Magnotta et al., 2012). Alterations in tissue pH also underlie many pathophysiological processes, such as ischemic stroke, epilepsy, and traumatic brain injury. Thus, a non-invasive pH-sensitive imaging tool can provide unique insight into the understanding of brain function as well as neurological and psychiatric disorders, and is also a prime target for diagnosis and evaluating response to treatment responses in many diseases (Duncan, 1997; Gerweck and Seetharaman, 1996; Sheth et al., 2012; Tannock and Rotin, 1989). For example, because tissue acidosis and viability are closely associated with oxygen and glucose metabolism (Anderson et al., 1999; Sun et al., 2007; Tomlinson et al., 1993), pH-imaging has been suggested as a metabolic biomarker for the salvageable penumbra in acute ischemic stroke (Astrup et al., 1981; Sako et al., 1985; Warach, 2001), complementing current clinical methods such as diffusion and perfusiom MRI.

Tissue pH has been measured non-invasively by magnetic resonance spectroscopy (MRS) or chemical shift imaging methods, with ^{31}P from the frequency separation between inorganic phosphate and phosphocreatine or ^{1}H from the lactate content, but the low sensitivity of these methods limits the spatial resolution. Moreover, significant signal averaging results in a temporal resolution too slow for many dynamic studies. The sensitivity to pH can be enhanced with a variant of the chemical exchange saturation transfer (CEST) MRI technique (Ward et al., 2000); this technique, commonly referred to as amide proton transfer (APT) (Sun et al., 2011a; Sun et al., 2011b; Sun et al., 2007; Zhou et al., 2003), selectively saturates the amide protons in the backbone of cytoplasmic proteins. These amide protons exchange with water, leading to a decrease in MR imaging signal which is highly pH-sensitive. In the core of ischemic stroke, APT contrast can result in a decrease of about 1–2% of the water signal (i.e., ~1–2 M water protons) (Guo et al., 2016; Zhou et al., 2003; Zong et al., 2014), two orders of magnitude higher than the increase of lactate content reported in stroke studies (Jokivarsi et al., 2007; Rehncrona et al., 1981; Wagner et al., 1992; Zong et al., 2014).

Under a saturation radiofrequency (RF) pulse at the amide frequency, i.e., ~3.6 ppm downfield from water, the water signal is reduced not only by the amide-proton exchange from mobile proteins, but also by the direct water saturation (DWS) and magnetization transfer contrast (MTC) from immobile macromolecules. To minimize the DWS and MTC effects, CEST generally utilizes two images that differ only in offset polarity (±Ω) and calculates the difference between these normalized image intensities (Zhou et al., 2003)

$$\mathrm{MTR}_{\mathrm{asym}}(\Omega, B_1)=\{S_{\mathrm{sat}}(-\Omega, B_1)-S_{\mathrm{sat}}(+\Omega, B_1)\}/S_0, \quad [1]$$

where S_{sat} and S_0 is the signal intensity with and without saturation, respectively. However, the *in vivo* MTC effect is asymmetric around the resonance frequency of water (Hua et al., 2007; Zhou et al., 2003), and thus cannot be fully removed. For amide-CEST (i.e., APT), the nuclear Overhauser effect (NOE) from aliphatic protons (which spans from about −0.5 to −5 ppm from the water frequency) also contributes to the signal (Jin et al., 2013). Thus, the measured signal is generally denoted as APT-weighted (APTw) (Zong et al., 2014):

$$\mathrm{APTw}=\mathrm{MTR}_{\mathrm{asym}}(3.6\mathrm{ppm})$$

While pH has little variation in normal brain tissues, APTw maps show large heterogeneity due to these confounding effects. The difference between APTw values in gray and white matter can be as larger as ~2.5% at 9.4 T (Jin et al., 2013), and similar difference has been reported at 4.7 T (Guo et al., 2016). This background contrast is larger than the acidosis-induced change of APTw signals at the severely acidotic ischemic core (~1.5 %) where local tissue pH decreases by 0.5–1.0 unit (Back et al., 1994; Bereczki and Csiba, 1993; Rehncrona, 1985). Note that the pH deficit for peri-core ischemic tissue, such as the ischemic penumbra, is much smaller and usually less than 0.1–0.2 units (Anderson et al., 1999; Peek et al., 1989). In many other pathophysiological states, the change in pH is also on the order of 0.1–0.2 units (Chesler and Kaila, 1992; Duncan, 1997; Garnett et al., 2001; Laxer et al., 1992; McIntosh et al., 1987), thus it is necessary to improve the pH-sensitivity of APTw for broader application of pH-imaging.

In this study, we propose a novel method to enhance the pH-sensitivity by combining the CEST effect from the amide and guanidyl groups, which will be referred to as pH_{enh}. This method exploits the fact that the guanidyl protons, which are abundant in side chains of cytoplasmic proteins/peptides, exchange with water proton at much faster rate (k) than amide (Liepinsh and Otting, 1996). Simulation, phantom, and *in vivo* studies were performed to evaluate the signal characteristics and the sensitivity of pH_{enh}, and compared with APTw.

Materials and Methods

Theoretical background

In contrast to the pH-sensitive CEST effect of amide at 3.6 ppm, the saturation induced signal decay at the reference image at −3.6 ppm is mostly due to the NOE and MTC effect and is pH-insensitive (Jin et al., 2013). Thus, we propose to replace this reference image with an image of guanidyl-CEST. Acidification under physiological conditions reduces the chemical exchange rate k between amide and water protons and decreases amide-CEST signal (Sun et al., 2011a; Sun et al., 2012; Sun et al., 2007; Tietze et al., 2014; Zhou et al., 2003). Acidification under physiological conditions also reduces k between guanidyl and water protons; however, with judicious selection of RF saturation power (B_1) by a process called B_1–tuning (Jin and Kim, 2012; Zong et al., 2014), tissue acidification may increase guanidyl-CEST signals. Thus, an enhancement of pH-sensitivity can be obtained by acquiring both amide- and guanidyl- CEST images, and subtracting them as

$$pH_{enh} = \{S_{\mathrm{sat}}(\alpha \times B_1, 3.6\,\mathrm{ppm}) - S_{\mathrm{sat}}(B_1, 2.0\,\mathrm{ppm})\}/S_0, \quad [2]$$

where α is the ratio of RF powers for saturation at Ω = 3.6 ppm and 2.0 ppm. When the frequency offset of the saturation pulse is close to the water, the DWS effect can be expressed as:

$$DWS \equiv 1 - S_{sat}/S_0 = 1 - \frac{1}{1 + (T_1/T_2)(\gamma B_1/\Omega)^2}, \quad [3]$$

where T_1 and T_2 are the longitudinal and transverse relaxation times of water. Thus, the DWS effect is related to the ratio of B_1 and Ω, and would be equal in the two CEST images in Eq. [2] if α is set to 1.8. This value is independent of B_0, T_1 and T_2. It should be emphasized that pH_{enh} is obtained from two downfield frequencies of 3.6 ppm and 2.0 ppm, while APTw from downfield 3.6 ppm and upfield −3.6 ppm.

Simulations

Three-pool exchange between free water protons, labile protons, and bound water protons were simulated by modified Bloch Equations where the lineshape of bound water was modeled by a super-Lorentzian function (Jin et al., 2013; Morrison et al., 1995). For the baseline condition, we assumed a bound water proton fraction (f_{MT}) of 0.08, the magnetization transfer rate between bound water and free water (k_{MT}) of 50 s^{-1}, and the fractions of amide (f_{amide}) and guanidyl ($f_{guanidyl}$) protons to be 0.001 and 0.0004, respectively. The T_1 (T_2) of water, labile proton, and bound water protons for 9.4 T were assumed to be 2 s (50 ms), 2 s (50 ms), and 2 s (15 μs), respectively. MTR_{asym}values were simulated from Eq. [1] as a function of *k* for different saturation power. The exchange rates of amide and guanidyl protons with water are pH-dependent, and have been reported as:

$$\begin{aligned} k_{amide} &= 5.57 \times 10^{pH-6.4}, \\ k_{guanidyl} &= 216 \times 10^{pH-6.4} \end{aligned} \quad [4]$$

where the 1st equation for amide was adopted from *in vivo* results (Zhou et al., 2003), and the 2nd equation for guanidyl was estimated from the *in vitro* results (Liepinsh and Otting, 1996). To estimate the contrast induced by a drop of pH from the normal tissue value of 7.1 (Zhou et al., 2003), the changes of pH_{enh} and MTR_{asym} for amide proton at 3.6 ppm and guanidyl proton at 2 ppm are calculated, assuming a drop of tissue pH of 0.1, 0.3, and 0.5 units (i.e., pH drops from 7.1 to 7.0, 6.8, and 6.6).

While pH_{enh} can provide pH-weighted imaging, similar to APTw, it is affected by many experimental and non-pH physiological factors. First, pH_{enh} is susceptible to the B_0 and B_1 inhomogeneities. The baseline APTw and pH_{enh} values, as well as the contrast of APTw and pH_{enh} caused by a drop of tissue pH of 0.1, 0.3, and 0.5 units, were simulated for a variation of B_0 from 0 to 40 Hz, and for a variation of B_1 of 0 to 30%. Secondly, pH_{enh} imaging is

affected by non-chemical exchange effects, such as MTC and R_1 (=1/T_1) relaxation. To evaluate the magnitude of these effects, we simulated the change of pH_{enh} caused by a variation from −30% to 30% in f_{MT} and R_1 independently. In many pathological conditions, these changes are often correlated. Thus, we also simulated the case where f_{MT} and R_1 changes together. Finally, because pH_{enh} signal is also dependent on the concentration of amide and guanidyl protons, the change of pH_{enh} signal caused by a variation from −30% to 30% in f_{amide} and/or $f_{guanidyl}$ were simulated. In the simulations above, the default B_1 was selected to be the same as our *in vivo* stroke experiments, i.e., 42 Hz for APTw, and 30 Hz at 2 ppm and 54 Hz at 3.6 ppm for pH_{enh}.

Animal Preparation

Thirteen male Sprague-Dawley rats weighing 252–385 g were studied with approval by the Institutional Animal Care and Use Committee at the University of Pittsburgh. The animals were anesthetized with isoflurane (5% for induction and 2% during surgery) in a mixture of O_2 and air gases with the O_2 concentration kept at about 30% throughout the experiment. The right femoral vein was catheterized for the delivery of maintenance fluid, and the femoral artery was catheterized to monitor the arterial blood pressure. Middle cerebral artery occlusion (MCAO) was carried out to induce permanent ischemia in the left hemisphere (Kiozumi et al., 1986). After surgery, the isoflurane level was reduced to 1.4–1.5 % during MRI scans. The dynamic blood pressure and end-tidal CO_2 were monitored. End-tidal CO_2 level was kept within 3.0 – 4.0% and the rectal temperature was maintained at 37.5 ± 1.0°C using a feedback-controlled heating pad.

MR experiments

All experiments were performed on a 9.4 T magnet equipped with an actively shielded 12-cm gradient system (Magnex, UK), interfaced to a DirectDrive 2 console (Agilent, Santa Clara, CA, USA). For phantom experiments, a 3.8-cm ID quadrature volume coil (Rapid Biomedical, OH, USA) provided RF transmission and detection. For *in vivo* studies, a detunable volume excitation (6.4-cm diameter) and surface receiver coil combination (2.2-cm diameter) (Nova Medical Inc, Massachusetts, USA) was used. Magnetic field homogeneity was optimized by localized shimming on a volume of interest using a 3-D gradient-echo automated shimming routine. For a typical shimming volume of ~ 20 mm × 20 mm × 6 mm for phantom and 14 mm × 9 mm × 9 mm for *in vivo* experiments, the water spectral linewidths were 5–10 Hz and 20–30 Hz, respectively. Therefore, no correction of B_0-inhomogeneity was performed in our study. The B_1 field was mapped for calibration of the transmit power (Jin and Kim, 2010). CEST images were acquired with a continuous wave saturation followed immediately by crushing gradients and spin-echo EPI acquisition, where the saturation duration and the repetition time is 5 s and 14 s for the phantom study, and 3.5 s and 4 s for all *in vivo* experiments, respectively.

Phantom experiments

Protamine phantoms were used to examine the effect of B_1-tuning for pH-contrast. Protamine is a small protein consisting of ~2/3 arginine with exchangeable guanidyl groups in the side chains, as well as amide protons in the backbone. 15 mg/ml protamine was dissolved in phosphate buffered saline (PBS) and titrated to pH values of 6.1, 6.4, 6.7, and

7.0, and a PBS only sample was prepared for comparison. 0.15 mM $MnCl_2$ was added to each sample so that the T_1 and T_2 are closer to *in vivo* values. Z-spectra of phantoms were measured at 37 °C from 6 ppm to −6 ppm, with continuous wave pulse power of 21 Hz and 38 Hz (=1.8×21 Hz). The images were acquired immediately with a single-shot spin-echo EPI sequence, where the field of view (FOV) = 40 mm × 40 mm, the matrix size = 64 × 64, slice thickness = 5 mm, the echo time = 28 ms.

In vivo experiments

To examine the sensitivity of pH_{enh}, two type of experiments were adopted to induce different level of acidosis: a dynamic studies with inhalation of 10% CO_2 which is expected to yield a pH drop of 0.1–0.2 unit in brain tissues (Magnotta et al., 2012; Nishimura et al., 1989), and an MCAO model where the pH drop is expected to be 0.5 to 1 unit in the ischemic core (Back et al., 1994; Bereczki and Csiba, 1993; Rehncrona, 1985).

Gas Challenge—APTw and pH_{enh} time series were acquired during hypercapnic and hyperoxic challenges (n = 4 rats). Hypercapnic or hyperoxic stimulations were achieved by inhalation of 10% CO_2 or 70% of O_2 for 5 min, respectively. The paradigm is 7 min baseline, 5 min challenge, and 15 min recovery. A time series of four images was acquired in an interleaved manner, with γB_1 = 34 Hz saturation applied at four offset frequencies of 3.6 ppm, −3.6 ppm, 2 ppm, and 300 ppm (used as S_0). The images were acquired by two-shot spin-echo EPI, where the FOV = 32 mm × 32 mm, the matrix size = 96 × 96, number of 2 mm-thick slices = 2, and the echo time = 8 ms. In each animal, data were averaged from three hypercapnic runs with a 1-h resting time between runs, and from two hyperoxic runs with 0.5-h resting time between runs.

Middle Cerebral Artery Occlusion—Two experiments were performed. First, *in vivo* Z-spectrum was measured between 1-h to 2-h post occlusion (n = 4), with saturation pulse of 34 Hz and at 75 offset values range between −12 to 12 ppm. The offsets were symmetric about water, but were spaced unevenly with steps of 0.1 ppm around the amide and guanidyl resonance frequencies, and wider space of 1 ppm between 6 ppm to 12 ppm and −6 ppm to −12 ppm. Three repetitions were averaged to increase the signal to noise ratio.

Second, for comparing pH-sensitivity between APTw and pH_{enh}, these maps were obtained ~2 h post the stroke onset (n = 5). For APTw studies, CEST was measured at offsets of −3.6 and 3.6 ppm, with saturation pulse power of 42 Hz. For pH_{enh} imaging, amide- and guanidyl-CEST were acquired with saturation of 30 Hz at 2.0 ppm and 54 Hz (=1.8 × 30 Hz) at 3.6 ppm, respectively, to match the DWS effect in Eq. [2]. A control (S_0) image was acquired with saturation applied at 300 ppm. Ten repetitions were averaged for APTw and pH_{enh} maps. All images were acquired by single-shot spin-echo EPI, where the FOV = 32 mm × 32 mm, the matrix size = 64 × 64, number of 2 mm-thick slices = 4, and the echo time = 30 ms. In addition, multi-slice apparent diffusion coefficient (ADC) maps were measured immediately after the CEST study, with a low *b*–value of 5 s/mm^2 applied on one axis, and a high *b*–value of 1500 s/mm^2 applied on six different directions.

In vivo data analysis

For the gas challenge study, time series of APTw and pH_{enh} ($\alpha = 1$) were calculated using Eq. [1] and [2], respectively. The Student's *t*-test was performed on a pixel-by-pixel basis on the time series of APTw or pH_{enh} maps to detect the area with significant changes. A box-car function was used where the baseline periods were selected as the 7 to 0 min before the challenge and 10 to 15 min after the challenge, and the stimulation period was selected as 2 to 6 min after the onset of challenge. A *p*-value threshold of < 0.05 was chosen (uncorrected for multiple comparisons), and a minimal cluster size of 4 pixels was applied for hypercapnia data, and 2 pixels for hyperoxia data.

For MCAO experiments, the ischemic core in the ipsilateral hemisphere was defined as areas with ADC values less than 77% of the normal contralateral side. The normal contralateral region of interest (ROI) was a mirror of the ipsilateral ischemic ROI across the midline, as shown below in the inset of Fig. 5. Sensitivity for the detection of pH-abnormalities with APTw or pH_{enh} map can be obtained from the contrast to noise ratio (CNR):

$$CNR = \frac{|CEST_i(\text{ipsi}) - CEST_i(\text{contra})|}{\sqrt{\sigma^2(\text{ipsi}) + \sigma^2(\text{contra})}} \quad [5]$$

where $CEST_i$ refers to APTw or pH_{enh} and σ is the standard deviation of the pixel values within the ipsi- or contralateral ROI.

Results

Computer Simulations

Fig. 1A shows the simulated MTR_{asym} as a function of *k* for two γB_1 values of 21 and 84 Hz. With these two power levels, the MTR_{asym} is tuned to an exchange rate ($k_{tune} = 2\pi \cdot \gamma B_1$) of 133 and 532 s^{-1}, respectively. The CEST contrast (change of MTR_{asym}) induced by tissue acidosis (i.e, decrease of *k*, indicated by green and pink arrows) can be either positive or negative, depending on the range of *k* values and the choice of γB_1. For amide protons with decreasing pH, the MTR_{asym} at 3.6 ppm decreased for most of the γB_1 range, and the optimal power was around 20 Hz (Fig. 1B). In contrast, for guanidyl protons, the MTR_{asym} increased at acidosis for most of the γB_1 values except large γB_1 of >90 Hz (Fig. 1C). The optimal power for a positive MTR_{asym} change was about 32 Hz to 40 Hz. Both amide- and guanidyl-CEST contrast were higher for a larger pH change. The pH_{enh} obtained by Eq. [2] with $\alpha = 1.8$ yields about 50% and 85% higher pH-contrast than the peak magnitude of amide- and guanidyl-CEST alone, respectively (Fig. 1D).

The effects of B_0 and B_1 variations to the APTw and pH_{enh} signals were simulated in Fig. 2. The baseline APTw and pH_{enh} signals both decrease with increasing variations in B_0 (Fig. 2A) and B_1 (Fig. 2B). While the B_0 variation leads to a larger error in the APTw than pH_{enh}, the B_1 variation leads to a larger error in the pH_{enh}. Both APTw and pH_{enh} contrasts caused by a drop in pH reduce due to B_0 and B_1 variations, but the relative effect is different for APTw and pH_{enh} contrasts (Fig. 2C and 2D). The absolute changes induced by acidosis were normalized by those without any B_0 and B_1 modulations, therefore, the normalized value of

1.0 does not have any error. For APTw, the normalized value induced by the B_0 and B_1 variation is similar for three levels of acidosis (dashed lines). For pH_{enh}, the normalized value is dependent on the acidosis level (solid lines), and is smaller than the APTw. These simulations demonstrate that baseline pH_{enh} is less (more) susceptible to B_0 (B_1) variations than APTw. Nonetheless, the acidosis-induced change of pH_{enh} is less sensitive to B_0 and B_1 inhomogeneity compared to APTw.

Fig. 3 shows the deviation of pH_{enh} caused by non-pH physiological changes. While pH_{enh} signals are sensitive to changes in f_{MT} and water R_1, their effects are similar in magnitude but opposite in direction, i.e., pH_{enh} is increased by a decrease of f_{MT} or an increase of R_1. Note in many pathological conditions, f_{MT} and R_1 are often well-correlated and changes in the same direction, thus, the total effect to pH_{enh} is determined by their difference. In the case when the percent changes are the same, the effect to pH_{enh} is nearly canceled out (red in Fig. 3A). Similarly, a decrease of f_{amide} and $f_{guanidyl}$ leads to opposite changes in pH_{enh}, thus the total effect would also be determined by their difference (Fig. 3B).

Phantom CEST Experiments

In protamine phantoms with pH = 6.4 and 7 (Fig. 4A), the Z-spectra measured with γB_1 = 38 Hz shows an example of opposite pH-induced contrast from the amide and guanidyl CEST effects (red versus green arrows). Note the DWS is larger when RF saturation is closer to the water proton resonance, as shown by comparing Z spectrum signal intensities of orange (Ω = −2.0 ppm) vs. pink (Ω = −3.6 ppm) arrows. In the MTR_{asym} spectra (Fig. 4B and 4C), a large guanidyl peak appears at 2 ppm, besides a smaller amide peak at 3.7 ppm. For both amide- and guanidyl-CEST (Fig. 4D and 4E), the MTR_{asym} is higher for a saturation pulse power of γB_1 = 38 Hz than 21 Hz. For amide-CEST, a decrease of pH (and the exchange rate) leads to a decrease of MTR_{asym} for both powers. For guanidyl-CEST, the MTR_{asym} increases monotonically with decreasing pH for 21 Hz, but reaches a peak at pH = 6.4 for 38 Hz. In Fig. 4F, the pH_{enh} increases the contrast between pH-phantoms. Note the pH_{enh} value was negative for the pH = 7 sample because protamine has a high concentration of guanidyl group, and thus, the guanidyl-CEST signal is larger than amide-CEST (Fig. 4B–C).

Fig. 5A shows the S_0 map of PBS phantom and three protamine phantoms with pH values denoted in red. The MTR_{asym} maps at 3.7 ppm and 2 ppm were measured with a saturation power of 38 Hz and 21 Hz, respectively (Fig. 5B and 5C). The opposite pH-dependence is clearly seen. Although guanidyl-CEST signal (*i.e.*, MTR_{asym} at 2 ppm) shows highest sensitivity for each individual protamine phantom, the contrast between the protamine phantoms is the largest with the pH_{enh} map (e.g., pH 6.1 vs. 6.4 samples, Fig. 5D). Note that the DWS effect is minimized in both MTR_{asym} maps, as shown by the PBS phantom in Fig. 5B and 5C. For pH_{enh}, the signal of PBS phantom is also minimized with the selection of α = 1.8 to match their DWS effect (Fig. 5D).

In vivo CEST Experiments

The *in vivo* pH-sensitivity of APTw and pH_{enh} was first compared in a dynamic study with a 34 Hz saturation power (Fig. 6). During 5 min of acidosis-inducing CO_2 challenge, the

APTw map shows only small signal drop, as shown by the blue-to-purple pixels in two of the brain slices. pH_{enh} detects a much larger signal increase, shown by the wide spread red-to-yellow pixels covering most of the cortex. Note that the CO_2 challenge also induces hemodynamic changes, such as increased CBF and blood volume. Thus, it is necessary to examine whether the pH_{enh} signal change is mainly due to the change in tissue pH, or can be induced by vascular responses. In Fig. 6C, no pH_{enh} response was detected under 70% O_2 challenge, which induces changes in CBF and blood volume but not pH (Lu et al., 2009), suggesting pH_{enh} response in Fig. 6B is mostly caused by tissue acidosis. Fig. 6D shows the average time course (n = 4) of APTw and pH_{enh} obtained from cortical ROIs. The peak signal change is around 0.55% and −0.18% of S_0 for pH_{enh} and APTw, respectively.

In rats with experimental stroke, saturation pulse with 34 Hz power was used to examine pH-induced changes in Z-spectra (n = 4). For quantitative comparison, ROIs were defined on ADC maps where these regions are outlined with solid contours for ischemic core on the ipsilateral side and dashed contours for normal tissue on the contralateral side (Inset, Fig. 7A). Z-spectra from ipsi- vs. contralateral ROIs showed opposite contrast for amide- (3.6 ppm; red arrow) vs. guanidyl-CEST (2.0 ppm; green arrow). Note that no change was observed in the NOE peak (−1 to −5 ppm; blue arrow). Despite the negative and distorted baseline in the MTR_{asym} spectra (Fig. 7B), the CEST signal in the low pH ishemic core was found to be reduced at around 3.6 ppm, but increased at 2 ppm.

In vivo pH_{enh} and APTw maps were also measured in stroke rats for comparing pH-sensitivity. pH_{enh} was obtained from guanidyl-CEST at 2.0 ppm acquired with 30 Hz and amide-CEST at 3.6 ppm acquired with 54 Hz (=1.8 × 30 Hz). For comparison, *in vivo* APTw maps were obtained with a 42 Hz saturation power which maximizes the APT contrast (Jin et al., 2013). In Fig. 8, the APTw map showed a negative baseline due to the NOE and asymmetric MTC effects, and hypointensive change in the ipsilateral hemishpere (left of images). Note that adjusting the gray scale can slightly improve the delineation of the ischemic lesion (Fig. 8A, left vs. right). A negative baseline was also observed in the pH_{enh} maps. While matching B_1/Ω balances the DWS, the MTC from semisolid macromolecules is unequal in these two images with 2.0 and 3.6 ppm saturation. Nonetheless, normal tissue showed smaller gray and white matter contrast in pH_{enh} maps than APTw maps. Tissue acidification appears hyperintense in pH_{enh} maps (in contrast to the hypointense appearance in APTw maps), and a threshold can be applied for better delineation of the lesion (Fig. 8B, left vs. right). The ischemic lesion identified by pH_{enh} maps matched closely with the ADC deficit, better than that of the APTw maps (purple versus red and yellow solid contours). The CEST contrast calculated from the difference between ipsi- and contralateral ROIs was −1.85 ± 0.42% for APTw and 3.04 ± 0.61% for pH_{enh} (n = 5, Fig. 8D). In addition to a higher CEST contrast, the pH_{enh} map also showed smaller spatial variations, i.e., smaller σ in both ipsilateral and contralateral ROIs. Consequently, the CNR of pH_{enh} calculated from Eq. [5] is about 2.9 ± 0.4 times higher than APTw.

Discussion

Conventional non-invasive MRI methods can assess a variety of information of biological tissues such as water content, iron content, water diffusion, blood flow and volume. Recent

developments of pH-weighted imaging provide novel information which is closely associated with oxygen/glucose metabolism, and thus, is complementary to current available methods and can assess disease extent and response to therapy for many pathological conditions, such as TBI, epilepsy and ischemic stroke. While pH-weighted imaging with APTw has been studied for more than one decade (Zhou et al., 2003), its utilization still faces significant technical challenges due to its poor pH-sensitivity. The signal change caused by pH-alteration is often lower than the inherent gray/white matter background contrast (Jin et al., 2013; Jones et al., 2013; Liu et al., 2013). In acute-stroke patients and animal stroke models, APTw can detect some signal differences between normal tissue and the severely-acidic infarct core; however, our results suggested that it is difficult to accurately delineate the pH-deficit regions. Robust detection of the mildly-acidotic ischemic penumbra would be even more difficult (Tee et al., 2014; Tietze et al., 2014), where the decrease in pH is expected to be only approximately 0.1–0.2 units (Anderson et al., 1999; Peek et al., 1989).

Many approaches have been proposed to minimize the confounding effects to APTw (Heo et al., 2016; Jin et al., 2013; Jones et al., 2012; Lee et al., 2013; Narvainen et al., 2010; Scheidegger et al., 2011; Song et al., 2012; Xu et al., 2014; Zaiss et al., 2011; Zu et al., 2013). In some of these approaches the sensitivity is sacrificed, such as the pulsed saturation scheme utilized in the chemical exchange rotation transfer approach (Zu et al., 2013) and the variable-delayed multi-pulse saturation approach (Xu et al., 2014). In others, many more data points should be acquired for post-acquisition analysis of multi-component data fitting which lengthens the acquisition (Heo et al., 2016; Jones et al., 2012; Zaiss et al., 2011). Our APT* method reduces these confounding effects and retains the APT sensitivity without significantly increasing the scanning time (Jin et al., 2013), but the application to lower clinical fields remains challenging because a distinct dip around the amide frequency in the Z-spectrum is more difficult to detect at lower fields.

Since the amide-water proton exchange is base-catalyzed under physiological conditions, APT effect decreases in acidosis and produce a negative contrast. Recently, we have shown that positive acidosis-contrast can be detected with amine proton exchange (APEX) approach (Jin et al., 2012). APEX signal is sensitive to the primary amine protons in amino acids and the side chain of cytoplasmic proteins, which has a chemical shift of 2.8 to 3 ppm from water and exchange with a rate of 5000 to 10000 s^{-1} with water protons at normal pH (Zong et al., 2014). The opposite change of amine- versus amide-CEST has also been exploited for mapping pH in stroke animals (McVicar et al., 2014). In this study, we showed that the positive contrast can also be obtained from the guanidyl groups with judicious selection of the saturation pulse power.

The CEST effect is determined by both the pH-depdenent chemical exchange rate and the labile proton concentration. Thus, a change in the total amide and guanidyl groups would also affect the pH_{enh} signal. It should be noted that these two groups have opposite effect on the pH_{enh} signal due to the subtraction used in Eq. [2], and hence, our simulation showed that a change of these two groups, if with similar magnitude, would lead to a negligible effect on the pH_{enh} contrast (Fig. 3). Therefore, a change in the mobile protein concentration, with amide groups in the backbone and guanidyl groups in the side chain,

will probably has minimal effect on pH_{enh} contrast. Compared to the APT effect, which mostly arises from mobile protein, it is known that the guanidyl-CEST signals have concentributions from mobile protein as well as creatine. It is usually accepted that in ischemic tissues the mobile protein concentration does not change within the initial hours (e.g., < 3 h) of stroke (Zhou et al., 2003); however, the creatine concentration may change slightly due to disrupted energy metabolism (Zong et al., 2014). Because creatine concentration is only 4–5 mM in healthy brain (Pouwels et al., 1999), we postulate that the majority of the guanidyl-CEST signal comes from mobile proteins, and a small change in creatine concentration during acute stroke (e.g., < 2 mM) should only have small impact on the pH_{enh} contrast. Nevertheless, further stroke studies to compare pH_{enh} imaging with MRS measurement of creatine, would be needed to examine this hypothesis.

Besides the guanidyl protons, there are other possible contributions to the endogenous CEST signal at 2.0 ppm, such as from the aromatic NOE from mobile proteins as suggested by our group and others (Jin and Kim, 2013; Zaiss et al., 2017), and amide of glutamine (Mori et al., 1998). Since NOE effects are insensitive to pH {Jin, 2013 #2715}, and amide has opposite pH-contrast with guanidyl with our selection of saturation powers, we expect that the pH-contrast at 2.0 ppm should be mostly from the guanidyl protons. Additionally, amine and hydroxyl protons with resonance frequencies close to 2.0 ppm may affect the guanidyl-CEST signal due to their fast exchange, but the contribution is expected to be small because of the low saturation power used here.

Recent study from our group and others suggested that MTR_{asym}, as an index of CEST sensitivity, is coupled to the MTC, DWS, and T_1 relaxation and is thus not a good index for quantification of the chemical exchange effect (Jin et al., 2011; Li et al., 2015). A relaxation rate based analysis with the removal of MTC, DWS, and T_1 effects may be more suitable for quantification of CEST effects (Jin et al., 2011; Li et al., 2015). However, this procedure requires acquisition of additional data which increases the overall scanning time. Since the goal of this study was to improve the sensitivity of pH-weighted imaging rather than to measure a quantitative pH change, we adopted the conventional MTR_{asym}-based analysis. An underlying assumption of our approach is that the total change caused by non-pH confounding effects should be small, so that the contrast mainly arises from a pH change. In our ischemic stroke data, this assumption holds well because the difference between Z-spectra of normal and ischemic region is minimal for all offset frequencies except near the amide and guanidyl frequencies (Fig. 7). Note that a decrease of f_{MT} and R_1, both expected in the ischemic core region, has opposite effects to the pH_{enh} contrast, and thus the toal effect would be determined by their difference.

In the pH_{enh} images, there is residual DWS contamination with the choice of $\alpha = 1.0$ (i.e., same B_1), such as in our gas challenge study in Fig. 6. While one concern is that the DWS may change during the challenge because of the BOLD effect, the minimal pH_{enh} change during hyperoxia challenge indicates that this effect should be negligible. In MCAO experiments, $\alpha = 1.8$ (in Eq. [2]) was selected to minimize the DWS contribution. However, since the MTC effect of immobile macromolecules differs at 2 and 3.6 ppm, contrast between gray and white matter still exists. Alternatively, α can be adjusted to reduce this residual gray and white matter contrast, so that the overall variation of pH_{enh} across the

brain pixels is minimized to further improve the CNR. A recent study suggested that MTC and relaxation-normalized APT analysis with additional acquisition of MTC and T_1 maps can reduce the background gray/white matter contrast of APTw, and thus, increase the pH-sensitivity (Guo et al., 2016). More research is necessary to compare the pH-sensitivity of these two approaches, and to examine whether similar correction approach can be incorporated with the pH_{enh} method to further improve the pH-sensitivity for acute stroke imaging.

Conclusion

We propose a pH-weighted MRI method by combining the CEST effects of the amide and guanidyl groups. The pH_{enh} approach exploits the different chemical exchange rate of guanidyl and amide protons. Its enhanced pH-sensitivity compared to APTw is confirmed by simulation, phantom and *in vivo* studies. By adjusting power and frequency offset of saturation pulses, pH_{enh} imaging is as easy to implement as APTw. We expect that pH_{enh} imaging can be a valuable tool for the study of many diseases such as stroke and traumatic brain injury. It may also be applied to dynamic studies such as neural activation and epilepsy.

Acknowledgments

We thank Kristy Hendrich for maintaining the 9.4 T system. This work is supported by NIH grants EB003324, P30-NS076405 and P30-CA047904, and the Institute for Basic Science in Korea (IBS-R015-D1).

References

Anderson RE, Tan WK, Martin HS, Meyer FB. Effects of glucose and PaO2 modulation on cortical intracellular acidosis, NADH redox state, and infarction in the ischemic penumbra. Stroke. 1999; 30:160–170. [PubMed: 9880405]

Astrup J, Siesjo BK, Symon L. Thresholds in cerebral ischemia - the ischemic penumbra. Stroke. 1981; 12:723–725. [PubMed: 6272455]

Autio JA, Shatillo A, Giniatullin R, Grohn OH. Parenchymal spin-lock fMRI signals associated with cortical spreading depression. Journal of Cerebral Blood Flow and Metabolism. 2014; 34:768–775. [PubMed: 24496172]

Back T, Hoehnberlage M, Kohno K, Hossmann KA. Diffusion nuclear magnetic resonance imaging in experimental stroke. Correlation with cerebral metabolites. Stroke. 1994; 25:494–500. [PubMed: 8303762]

Bereczki D, Csiba L. Spatial and temporal changes in tissue pH and ATP distribution in a new model of reversible focal forebrain ischemia in the rat. Metabolic Brain Disease. 1993; 8:125–135. [PubMed: 8272025]

Chesler M. Regulation and modulation of pH in the brain. Physiological Reviews. 2003; 83:1183–1221. [PubMed: 14506304]

Chesler M, Kaila K. Modulation of Ph by Neuronal-Activity. Trends in Neurosciences. 1992; 15:396–402. [PubMed: 1279865]

Duncan JS. Imaging and epilepsy. Brain. 1997; 120:339–377. [PubMed: 9117380]

Garnett MR, Corkill RG, Blamire AM, Rajagopalan B, Manners DN, Young JD, Styles P, Cadoux-Hudson TAD. Altered cellular metabolism following traumatic brain injury: A magnetic resonance spectroscopy study. Journal of Neurotrauma. 2001; 18:231–240. [PubMed: 11284544]

Gerweck LE, Seetharaman K. Cellular pH gradient in tumor versus normal tissue: Potential exploitation for the treatment of cancer. Cancer Research. 1996; 56:1194–1198. [PubMed: 8640796]

Guo Y, Zhou IY, Chan ST, Wang Y, Mandeville ET, Igarashi T, Lo EH, Ji X, Sun PZ. pH-sensitive MRI demarcates graded tissue acidification during acute stroke — pH specificity enhancement with magnetization transfer and relaxation-normalized amide proton transfer (APT) MRI. Neuroimage. 2016; 141:242–249. [PubMed: 27444569]

Heo HY, Zhang Y, Lee DH, Hong XH, Zhou JY. Quantitative Assessment of Amide Proton Transfer (APT) and Nuclear Overhauser Enhancement (NOE) Imaging with Extrapolated Semi-Solid Magnetization Transfer Reference (EMR) Signals: Application to a Rat Glioma Model at 4.7 Tesla. Magnetic Resonance in Medicine. 2016; 75:137–149. [PubMed: 25753614]

Hua J, Jones CK, Blakeley J, Smith SA, van Zijl PCM, Zhou JY. Quantitative description of the asymmetry in magnetization transfer effects around the water resonance in the human brain. Magnetic Resonance in Medicine. 2007; 58:786–793. [PubMed: 17899597]

Jin T, Autio J, Obata T, Kim SG. Spin-locking versus chemical exchange saturation transfer MRI for investigating chemical exchange process between water and labile metabolite protons. Magnetic Resonance in Medicine. 2011; 65:1448–1460. [PubMed: 21500270]

Jin T, Kim SG. Change of the cerebrospinal fluid volume during brain activation investigated by T1ρ-weighted fMRI. Neuroimag. 2010; 51:1378–1383.

Jin T, Kim SG. Quantitative chemical exchange sensitive MRI using irradiation with toggling inversion preparation. Magnetic Resonance in Medicine. 2012; 68:1056–1064. [PubMed: 22887701]

Jin, T., Kim, SG. In vivo saturation transfer imaging of nuclear overhauser effect from aromatic and aliphatic protons: implication to APT quantification. Proceedings of 21st Annual Meeting of ISMRM; Salt Lake City, Utah, USA. 2013. p. 2528

Jin T, Wang P, Zong X, Kim SG. MR imaging of the amide-proton transfer effect and the pH-insensitive nuclear overhauser effect at 9.4 T. Magnetic Resonance in Medicine. 2013; 69:760–770. [PubMed: 22577042]

Jokivarsi KT, Grohn HI, Grohn OH, Kauppinen RA. Proton transfer ratio, lactate, and intracellular pH in acute cerebral ischemia. Magnetic Resonance in Medicine. 2007; 57:647–653. [PubMed: 17390356]

Jones CK, Huang A, Xu JD, Edden RAE, Schar M, Hua J, Oskolkov N, Zaca D, Zhou JY, McMahon MT, Pillai JJ, van Zijl PCM. Nuclear Overhauser enhancement (NOE) imaging in the human brain at 7 T. Neuroimage. 2013; 77:114–124. [PubMed: 23567889]

Jones CK, Polders D, Huang W, Zhu H, Hoogduin HJ, Zhou JY, Luijten P, Van Zijl P. in vivo three-dimensional whole-brain pulsed steady-state chemical exchange saturation transfer at 7 T. Magnetic Resonance in Medicine. 2012; 67:1579–1589. [PubMed: 22083645]

Kiozumi J, Yoshida Y, Nakazawa T, Ooneda G. Experimental studies of ischemic brain edema: I: a new experimental model of cerebral embolism in rats in which recirculation can be introduced in the ischemic area. The Japanese Journal of Stroke. 1986; 8:1–8.

Laxer KD, Hubesch B, Sappeymarinier D, Weiner MW. Increased pH and inorganic phosphate in temporal seizure foci demonstrated by 31P MRS. Epilepsia. 1992; 33:618–623. [PubMed: 1628574]

Lee JS, Parasoglou P, Xia D, Jerschow A, Regatte RR. Uniform magnetization transfer in chemical exchange saturation transfer magnetic resonance imaging. Scientific Reports. 2013:3.

Li H, Zu ZL, Zaiss M, Khan IS, Singer RJ, Gochberg DF, Bachert P, Gore JC, Xu JZ. Imaging of amide proton transfer and nuclear Overhauser enhancement in ischemic stroke with corrections for competing effects. NMR in Biomedicine. 2015; 28:200–209. [PubMed: 25483870]

Liepinsh E, Otting G. Proton exchange rates from amino acid side chains - Implications for image contrast. Magnetic Resonance in Medicine. 1996; 35:30–42. [PubMed: 8771020]

Liu D, Zhou J, Xue R, Zuo Z, An J, Wang JJ. Quantitative characterization of nuclear Overhauser enhancement and amide proton transfer effects in the human brain at 7 tesla. Magnetic Resonance in Medicine. 2013; 70:1070–1081. [PubMed: 23238951]

Lu J, Dai GP, Egi Y, Huang S, Kwon SJ, Lo EH, Kim YR. Characterization of cerebrovascular responses to hyperoxia and hypercapnia using MRI in rat. Neuroimag. 2009; 45:1126–1134.

Magnotta VA, Heo HY, Dlouhy BJ, Dahdaleh NS, Follmer RL, Thedens DR, Welsh MJ, Wemmie JA. Detecting activity-evoked pH changes in human brain. Proc Nat Acad Sci. 2012; 109:8270–8273. [PubMed: 22566645]

McIntosh TK, Faden AI, Bendall MR, Vink R. Traumatic Brain Injury in the Rat: Alterations in Brain Lactate and pH as Characterized by 1H and 31P Nuclear Magnetic Resonance. Journal of Neurochemistry. 1987; 49:1530–1540. [PubMed: 3668537]

McVicar N, Li AX, Goncalves DF, Bellyou M, Meakin SO, Prado MAM, Bartha R. Quantitative tissue pH measurement during cerebral ischemia using amine and amide concentration-independent detection (AACID) with MRI. Journal of Cerebral Blood Flow and Metabolism. 2014; 34:690–698. [PubMed: 24496171]

Mori S, Eleff SM, Pilatus U, Mori N, van Zijl PCM. Proton NMR spectroscopy of solvent-saturable resonances: A new approach to study pH effects in situ. Magnetic Resonance in Medicine. 1998; 40:36–42. [PubMed: 9660550]

Morrison C, Stanisz GJ, Henkelman RM. Modeling magnetization transfer for biological-like systems using a semi-solid pool with super-Lorentzian lineshape and dipolar reservoir. Journal of Magnetic Resonance Series B. 1995; 108:103–113. [PubMed: 7648009]

Narvainen J, Hubbard PL, Kauppinen RA, Morris GA. Z-spectroscopy with Alternating-Phase Irradiation. Journal of Magnetic Resonance. 2010; 207:242–250. [PubMed: 20920868]

Nishimura M, Johnson DC, Hitzig BM, Okunieff P, Kazemi H. EFFECTS OF HYPERCAPNIA ON BRAIN PHI AND PHOSPHATE METABOLITE REGULATION BY P-31-NMR. Journal of Applied Physiology. 1989; 66:2181–2188. [PubMed: 2501277]

Peek KE, Lockwood AH, Izumiyama M, Yap EWH, Labove J. Glucose metabolism and acidosis in the metabolic penumbra of rat brain. Metabolic Brain Disease. 1989; 4:261–272. [PubMed: 2601642]

Pouwels PJW, Brockmann K, Kruse B, Wilken B, Wick M, Hanefeld F, Frahm J. Regional age dependence of human brain metabolites from infancy to adulthood as detected by quantitative localized proton MRS. Pediatric Research. 1999; 46:474–485. [PubMed: 10509371]

Rehncrona S. Brain Acidosis. Annals of Emergency Medicine. 1985; 14:770–776. [PubMed: 3927794]

Rehncrona S, Rosen I, Siesjo BK. Brain lactic acidosis and ischemic cell damage: 1. Biochemistry and neurophysiology Journal of Cerebral Blood Flow and Metabolism. 1981; 1:297–311. [PubMed: 7328145]

Sako K, Kobatake K, Yamamoto YL, Diksic M. Correlation of local cerebral blood flow, glucose utilization, and tissue pH following a middle cerebral artery occlusion in the rat. Stroke. 1985; 16:828–834. [PubMed: 4049447]

Scheidegger R, Vinogradov E, Alsop D. Amide proton transfer imaging with improved robustness to magnetic field inhomogeneity and magnetization transfer asymmetry using Saturation with Frequency Alternating RF Irradiation. Magnetic Resonance in Medicine. 2011; 66:1275–1285. [PubMed: 21608029]

Sheth VR, Li YG, Chen LQ, Howison CM, Flask CA, Pagel MD. Measuring in vivo tumor pHe with CEST-FISP MRI. Magnetic Resonance in Medicine. 2012; 67:760–768. [PubMed: 22028287]

Song XL, Gilad AA, Joel S, Liu GS, Bar-Shir A, Liang YJ, Gorelik M, Pekar JJ, van Zijl PCM, Bulte JWM, McMahon MT. CEST phase mapping using a length and offset varied saturation (LOVARS) scheme. Magnetic Resonance in Medicine. 2012; 68:1074–1086. [PubMed: 22246684]

Sun PZ, Cheung JS, Wang EF, Lo EH. Association between pH-weighted endogenous amide proton chemical exchange saturation transfer MRI and tissue lactic acidosis during acute ischemic stroke. Journal of Cerebral Blood Flow and Metabolism. 2011a; 31:1743–1750. [PubMed: 21386856]

Sun PZ, Wang EF, Cheung JS. Imaging acute ischemic tissue acidosis with pH-sensitive endogenous amide proton transfer (APT) MRI-Correction of tissue relaxation and concomitant RF irradiation effects toward mapping quantitative cerebral tissue pH. Neuroimage. 2012; 60:1–6. [PubMed: 22178815]

Sun PZ, Wang EF, Cheung JS, Zhang XA, Benner T, Sorensen AG. Simulation and Optimization of Pulsed Radio Frequency Irradiation Scheme for Chemical Exchange Saturation Transfer (CEST) MRI-Demonstration of pH-Weighted Pulsed-Amide Proton CEST MRI in an Animal Model of Acute Cerebral Ischemia. Magnetic Resonance in Medicine. 2011b; 66:1042–1048. [PubMed: 21437977]

Sun PZ, Zhou JY, Sun WY, Huang J, van Zijl PCM. Detection of the ischemic penumbra using pH-weighted MRI. Journal of Cerebral Blood Flow and Metabolism. 2007; 27:1129–1136. [PubMed: 17133226]

Tannock IF, Rotin D. Acid pH in tumors and its potential for therapeutic exploitation. Cancer Research. 1989; 49:4373–4384. [PubMed: 2545340]

Tee YK, Harston GWJ, Blockley N, Okell TW, Levman J, Sheerin F, Cellerini M, Jezzard P, Kennedy J, Payne SJ, Chappell MA. Comparing different analysis methods for quantifying the MRI amide proton transfer (APT) effect in hyperacute stroke patients. NMR in Biomedicine. 2014; 27:1019–1029. [PubMed: 24913989]

Tietze A, Blicher J, Mikkelsen IK, Ostergaard L, Strother MK, Smith SA, Donahue MJ. Assessment of ischemic penumbra in patients with hyperacute stroke using amide proton transfer (APT) chemical exchange saturation transfer (CEST) MRI. NMR in Biomedicine. 2014; 27:163–174. [PubMed: 24288260]

Tomlinson FH, Anderson RE, Meyer FB. Brain pHi, cerebral blood flow, and NADH fluorescence during severe incomplete global ischemia in rabbits. Stroke. 1993; 24:435–443. [PubMed: 8446980]

Wagner KR, Kleinholz M, Decourtenmyers GM, Myers RE. Hyperglycemic versus normoglycemic stroke: topography of brain metabolites, intracellular pH, and infarct size. Journal of Cerebral Blood Flow and Metabolism. 1992; 12:213–222. [PubMed: 1548294]

Warach S. Tissue viability thresholds in acute stroke - The 4-factor model. Stroke. 2001; 32:2460–2461. [PubMed: 11692000]

Ward KM, Aletras AH, Balaban RS. A new class of contrast agents for MRI based on proton chemical exchange dependent saturation transfer (CEST). Journal of Magnetic Resonance. 2000; 143:79–87. [PubMed: 10698648]

Xu J, Yadav NN, Bar-Shir A, Jones CK, Chan KW, Zhang J, Walczak P, McMahon MT, van Zijl PCM. Variable delay multi-pulse train for fast chemical exchange saturation transfer and relayed-nuclear overhauser enhancement MRI. Magnetic Resonance in Medicine. 2014; 71:1798–1812. [PubMed: 23813483]

Zaiss M, Schmitt B, Bachert P. Quantitative separation of CEST effect from magnetization transfer and spillover effects by Lorentzian-line-fit analysis of z-spectra. Journal of Magnetic Resonance. 2011; 211:149–155. [PubMed: 21641247]

Zaiss M, Windschuh J, Goerke S, Paech D, Meissner JE, Burth S, Kickingereder P, Wick W, Bendszus M, Schlemmer HP, Ladd ME, Bachert P, Radbruch A. Downfield-NOE-suppressed amide-CEST-MRI at 7 Tesla provides a unique contrast in human glioblastoma. Magnetic Resonance in Medicine. 2017; 77:196–208. [PubMed: 26845067]

Zhou JY, Payen JF, Wilson DA, Traystman RJ, van Zijl PCM. Using the amide proton signals of intracellular proteins and peptides to detect pH effects in MRI. Nature Medicine. 2003; 9:1085–1090.

Zong X, Wang P, Kim SG, Jin T. Sensitivity and Source of Amine-Proton Exchange and Amide-Proton Transfer Magnetic Resonance Imaging in Cerebral Ischemia. Magnetic Resonance in Medicine. 2014; 71:118–132. [PubMed: 23401310]

Zu ZL, Janve VA, Xu JZ, Does MD, Gore JC, Gochberg DF. A new method for detecting exchanging amide protons using chemical exchange rotation transfer. Magnetic Resonance in Medicine. 2013; 69:637–647. [PubMed: 22505325]

Highlights

- The pH_{enh} MRI combines the amide- and guanidyl-CEST effects to enhance the pH-sensitivity.
- With B_1-tuning, acidosis induce a negative and a positive contrast for the amide- and guanidyl-CEST signal, respectively.
- In pH_{enh}, the RF powers are also adjusted to match the direct water saturation at amide and guanidyl frequencies.
- Phantom and *in vivo* studies confirm a higher pH-sensitivity for pH_{enh} over APT-weighted MRI.

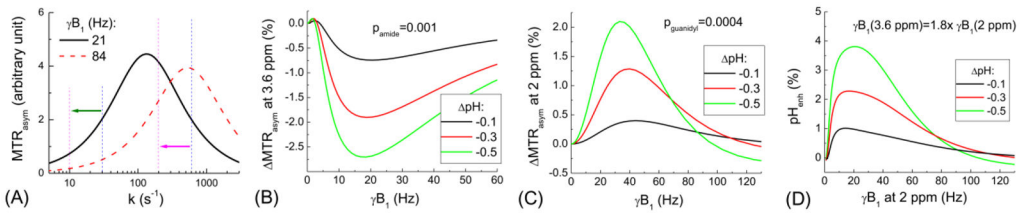

Fig. 1. B_1–tuning of the CEST contrast: Bloch simulations

(**A**) MTR_{asym} was simulated as a function of exchange rate (k) for two γB_1 levels of 21 and 84 Hz. Note that MTR_{asym} is tuned to $k = 2\pi\gamma B_1$. Assuming a decrease of k from 600 to 200 s^{-1} (pink arrow), simulation results show that the MTR_{asym} measured with γB_1 = 21 or 84 Hz would increase or decrease, respectively. If k decreases from 30 to 10 s^{-1} (green arrow), MTR_{asym} decreases for both B_1 levels. (**B**) The change of MTR_{asym} at 3.6 ppm induced by tissue acidosis as a function of γB_1 shows a decrease of amide-CEST signal for nearly all the γB_1 range. (**C**) The change of MTR_{asym} at 2 ppm during acidosis as a function of γB_1 shows an increase of guanidyl-CEST signal. (**D**) The pH contrast can be enhanced with pH_{enh} which combines the amide- and guanidyl-CEST effects. To balance the direct water saturation at two different frequencies, different power levels are used.

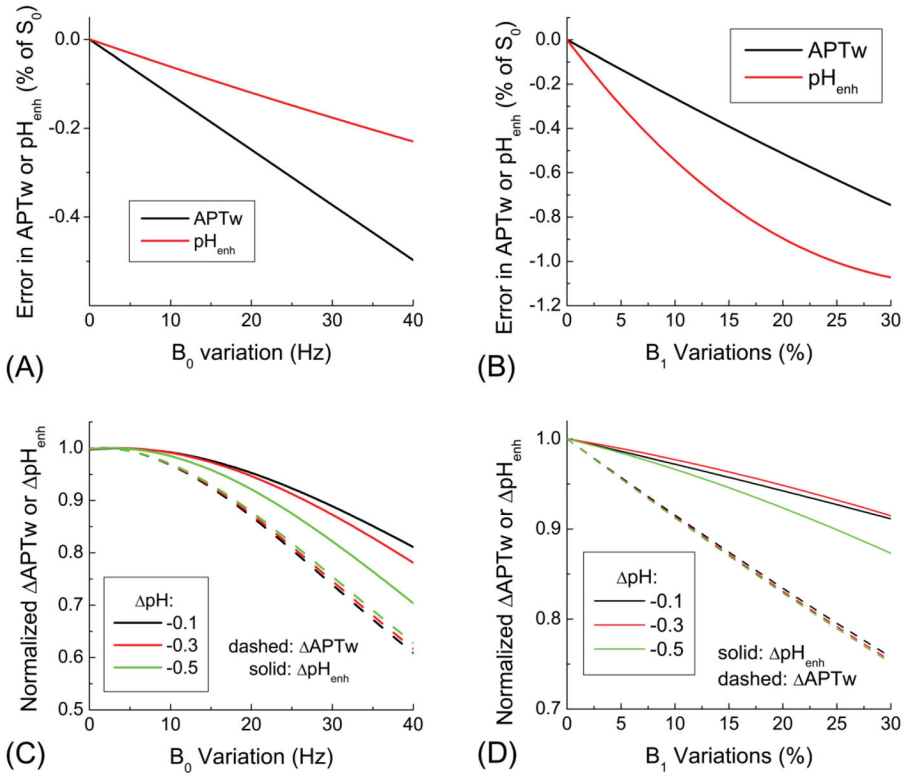

Fig. 2. Effect of B_0 and B_1 variations on pH_{enh} and APTw signals

The absolute error induced by B_0 and B_1 variations was determined for baseline conditions, while the normalized change was determined as a results of tissue acidosis. The baseline signal drift is less (more) sensitive to B_0 (B_1) for pH_{enh} **(A–B)**. In the presence of B_0 and B_1 variations, changes of APTw and pH_{enh} signals due to tissue acidosis reduce, and the normalized change is smaller for pH_{enh} than APTw **(C–D)**.

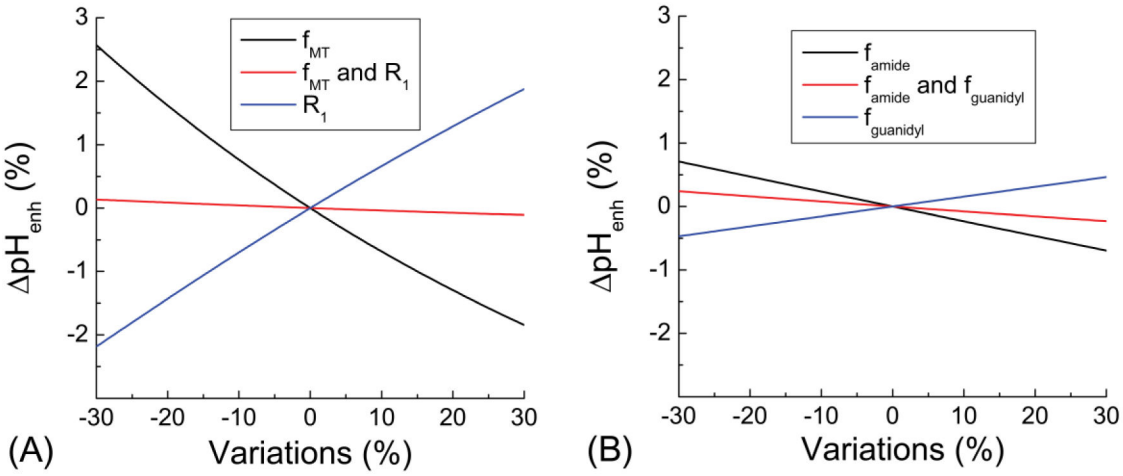

Fig. 3. Contribution of non-pH physiological changes to pH_{enh}

Fraction of semi-solid macromolecule protons (f_{MT}), amide (f_{amide}), and guanidyl protons ($f_{guanidyl}$) may be changed in diseased conditions as well as water relaxation time. These effects to pH $_{enh}$ signals were simulated. (**A**) A change of f_{MT} or water R_1 leads to opposite changes in the pH_{enh} signal. Hence, when f_{MT} and water R_1 both change similarly, its effect to pH_{enh} almost cancels out. (**B**) An increase of f_{amide} or $f_{guanidyl}$ leads to opposite changes in the pH_{enh} signal. When f_{amide} and $f_{guanidyl}$ both change with same percentage, its effect to pH_{enh} almost cancels out.

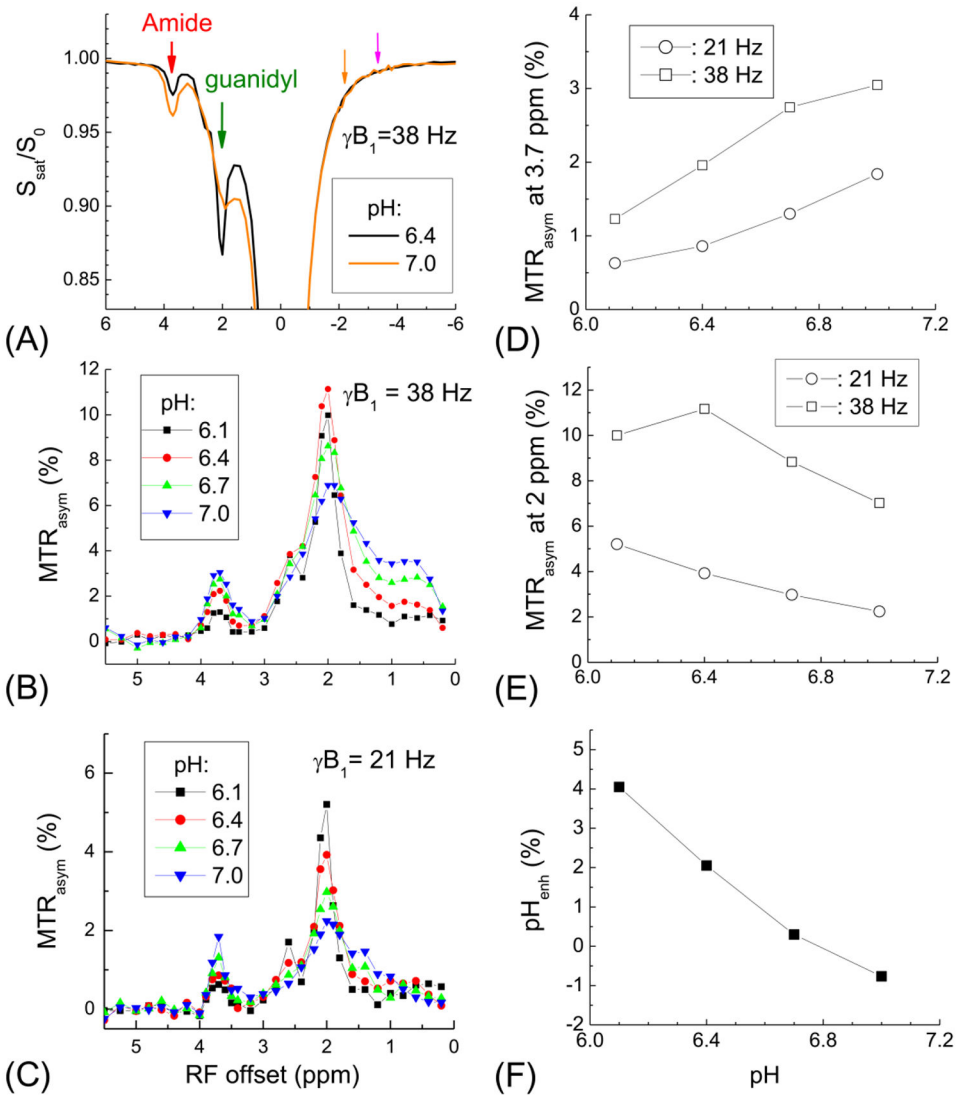

Fig. 4. pH sensitivity of amide and guanidyl CEST contrast: protamine phantom experiments

(**A**) Z-spectra of protamine phantoms with pH of 6.4 and 7.0 were measured with γB_1 = 38 Hz. The CEST signal from amide (red arrow) and guanidyl (green arrow) protons has opposite changes between two pH phantoms. These two CEST signals contain different contribution from the DWS, as shown by the pink and orange arrows at the opposite side of the water frequency. MTR_{asym} was measured with γB_1 = 38 Hz (**B**) and 21 Hz (**C**) for protamine phantoms at four different pH values, showing peaks at 3.7 ppm for the amide and 2 ppm for the guanidyl-CEST signals. Peak magnitude of MTR_{asym} for amide-CEST at 3.7 ppm (**D**) and guanidyl-CEST at 2 ppm (**E**) show different pH- and power-dependences. (**F**) pH_{enh} obtained from 21 Hz guanidyl and 38 Hz amide peaks enhances the contrast among these phantoms.

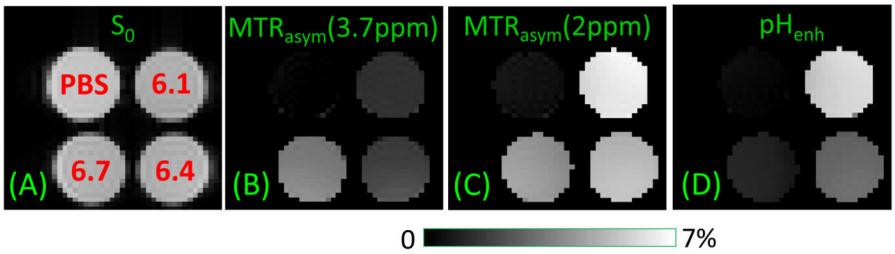

Fig. 5. pH contrast of MTR_{asym} vs. pH_{enh} in protamine phantoms

PBS phantom and three protamine phantoms (denoted in red in A) with pH = 6.1, 6.4, and 6.7 were used for pH sensitivity. A SE-EPI image is used as S_0 (**A**). MTR_{asym} maps of amide-CEST at 3.7 ppm (**B**) and the guanidyl-CEST at 2 ppm (**C**), with 38 Hz and 21 Hz saturation pulse power, respectively, show opposite pH-contrasts between different protamine phantoms. (**D**) With pH_{enh}, the contrast between protamine phantoms with different pH phantoms is larger than both the MTR_{asym} maps at 3.7 and 2 ppm.

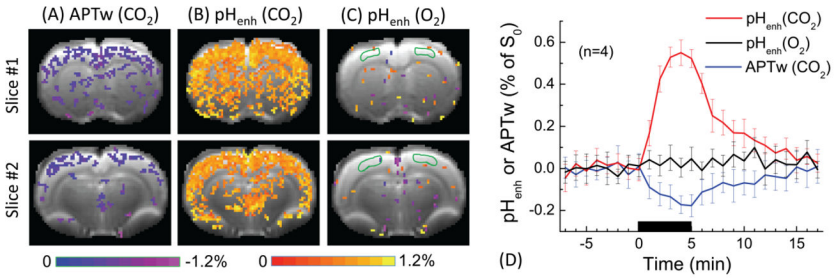

Fig. 6. ***In vivo*** **APTw vs. pH_{enh} results of hypercapnia and hyperoxia challenge**

10% CO_2 gas was used to induce tissue acidosis and 70% O_2 gas was used as a control experiment. Percent change maps of (**A**) APTw and (**B**) pH_{enh} induced by 10% CO_2 challenge, and (**C**) pH_{enh} during 70% O_2 challenge were overlaid on EPI images. (**D**) Time courses were obtained from the cortical ROI (delineated in C by green countours). Error bars: SD (n = 4), the black horizontal bar, time of gas challenge. During the acidosis-inducing CO_2 challenge, APTw signal decreases slightly, whereas pH_{enh} shows a much larger signal increase. In a control experiment, pH_{enh} shows a minimal response during O_2 challenge, which induces blood flow and volume changes without acidosis.

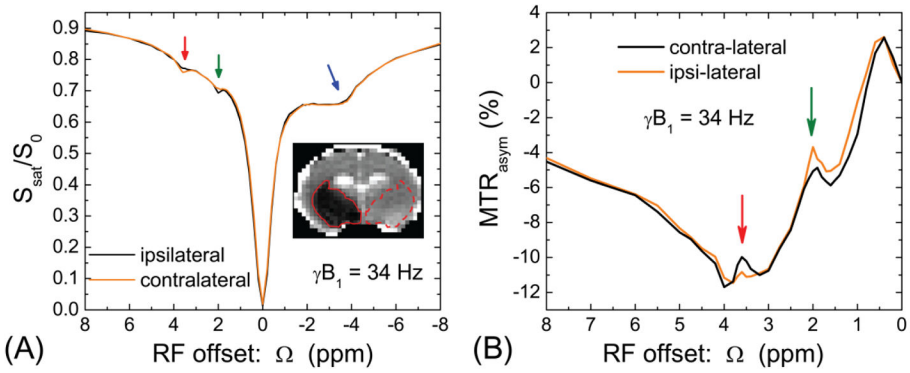

Fig. 7. ***In vivo*** **Z-spectra and MTR_{asym}-spectra from rat brain with MCAO**

Z-spectra with a saturation power of 34 Hz were obtained from rat brains with ischemic region (n = 4). The ipsilateral (solid contour) and contralateral (dashed contour) ROIs were selected based on the ADC map (Inset). (**A**) Z-spectra obtained from two ROIs are similar for most of the frequency range, except small changes at the amide and guanidyl frequencies. (**B**) The MTR_{asym}-spectra showed that the ipsilateral ischemic region has reduced amide-CEST and enhanced guanidyl-CEST signals. Note that other signals in the Z-spectra are insensitive to ischemia, such as from aliphatic protons or the MTC effect.

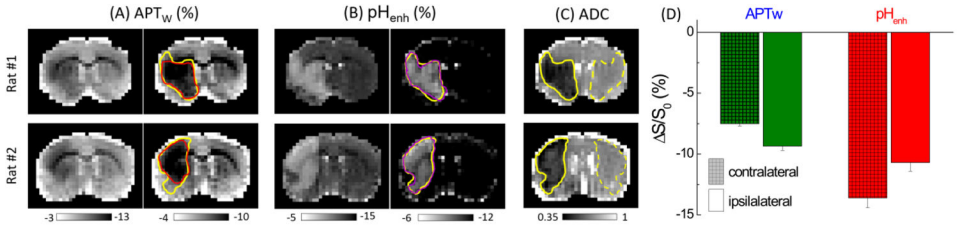

Fig. 8. *In vivo* APTw vs. pH_{enh} results from rat brain with MCAO

(A–B) APTw and pH_{enh} from two rat brains measured at 2 h post MCAO were shown with two different scale bars of 10% and 6% of contrast. (**C**) Respective ADC maps showed the ischemic core region in the ipsilateral hemisphere. Due to the large background heterogeneity of APTw, clear delineation of ischemic lesion is problematic, and its identified lesion area (red) is smaller than that of the ADC map (yellow). Compared to the negative contrast of APTw, the lesion can be better identified with the positive contrast of pH_{enh}, which matches well with the ADC map. With appropriate thresholding, the lesion area can be determined in the pH_{enh} map, except pixels at the ventricle region and at the boundary of the brain. (**D**) The magnitude of contrast between ipsilateral and contralateral ROIs, defined in the ADC maps as dashed and solid contours, respectively, is higher for pH_{enh} than that for APT_W.